AIAA JOURNAL
Vol. 46, No. 1, January 2008

Optimal Placement of Constrained-Layer Damping for Reduction of Interior Noise

D.-H. Lee*
Dongeui University, Busan 614-714, Republic of Korea

DOI: 10.2514/1.30648

In this paper, an efficient constrained-layer damping layout optimization method in structural-acoustic systems is proposed. To simulate vibro-acoustic systems, a hybrid model that uses finite elements for structures and boundary elements for the cavity is developed. With a finite element formulation, the intrinsic nonlinearities of viscoelastic damping materials with respect to frequency and temperature are included using a fractional–derivative model. The resulting complex eigenvalue problem is solved using an iterative scheme. The optimal layout of the constrained viscoelastic layer damping on the structure is identified using a gradient-based numerical search algorithm. The sensitivity formulas are derived analytically for acoustic and structural responses. The optimal damping-layer layouts that minimize the added mass with minimum sound pressure level requirements are obtained for different temperatures.

Nomenclature

$\boldsymbol{A}$	=	system matrix of boundary element
a_k	=	modal coordinate of kth mode
$\boldsymbol{B}$	=	system matrix of boundary element
$\boldsymbol{b}$	=	design variables
$\boldsymbol{E}$	=	complex modulus
$\boldsymbol{F}$	=	force vector
f	=	frequency, Hz
$\boldsymbol{G}$	=	shear modulus
h_1	=	thickness of base beam
h_2	=	thickness of damping layer
h_3	=	thickness of constraining layer
$\boldsymbol{i}$	=	unit imaginary number,$=\sqrt{-1}$
$\boldsymbol{K}$	=	stiffness matrix
k_i	=	generalized modal stiffness of ith mode
L	=	length of constrained-layer damping
$\boldsymbol{M}$	=	mass matrix
m_i	=	generalized modal mass of ith mode
$\boldsymbol{P}$	=	nodal sound pressure vector
$\boldsymbol{p}$	=	sound pressure
T	=	temperature
$\boldsymbol{V}_n$	=	nodal normal component of boundary velocity vector
$\boldsymbol{v}$	=	velocity vector
$\boldsymbol{x}$	=	displacement vector
$\boldsymbol{y}$	=	complex eigenvector
α	=	shift factor
η_k	=	loss factor of kth mode
κ	=	wave number
λ	=	complex eigenvalue
μ_k	=	natural frequency of kth mode
ξ	=	position vector
ρ	=	density
ω	=	angular velocity, $=2\pi f$

Presented as Paper 6918 at the 11th AIAA/ISSMO Multidisciplinary Analysis and Optimization Conference, Portsmouth, Virginia, 6–8 September 2006; received 23 February 2007; revision received 21 July 2007; accepted for publication 25 August 2007.

*Associate Professor, Department of Mechanical Engineering, 995 Eomgwangno, Busanjin-gu; dooho@deu.ac.kr.

I. Introduction

THERE are several techniques that can be used to suppress mechanical vibration and noise [1]. Among them, the addition of damping is one of the most practical approaches over a wide range of applications from transportation to structures. In particular, a surface treatment of viscoelastic damping materials on a structure is a conventional method to reduce structural vibrations or interior noises owing to the low cost and easy implementation of such a treatment [2]. For example, on the body structure of passenger cars, many damping sheets are attached for the purpose of reducing noise and vibration of the cabin. One can also see similar cases in airplanes, launch vehicles, ships, and electric appliances. However, the addition of damping inevitably increases the weight of the host structure. This should be minimized, as a reduction of weight generally results in both performance and economic benefits. In an effective treatment of damping materials, it is very important to determine the location, thicknesses, and shape of damping sheets. Such determinations are related to the design parameters of a damping treatment.

In many cases, a full treatment of surface damping does not give maximum damping for structures [1,3]. There are two types of surface damping: the first is known as the unconstrained type and the second the constrained type. Constrained damping has a high loss factor because it dissipates energy during the shear deformation of viscoelastic materials generated by a constraining metal layer. After Plunkett and Lee [4] investigated the optimal length of partial surface damping treatments theoretically, many researchers examined optimal design problems related to constrained [5–10] or unconstrained [11,12] layer damping in an effort to obtain the maximum loss factor or the minimum responses of a structure. Recently, research interests on surface damping treatment have explored damping-layout solutions to control various interior noise or radiation problems. Kruger and Mann [3] showed the importance of the optimal placement of constrained-layer damping patches in controlling noise problems by combining experimental measurements, boundary-element analysis, and a simulated annealing method. Azzouz and Ro [13] determined the optimal placement of passive constrained-layer damping using a structural intensity approach and finite element modeling to maximize the performance of active constrained-layer damping for a plate/cavity system. Similarly, Gibbs and Cabell [14] proposed an optimal placement method using a constrained-layer damping patch in regions of maximum curvature for a selected mode to enhance the performance of a sound-radiation controller. Zheng and Cai [15] conducted an optimization study of constraining-layer damping to minimize the sound power radiated by a simply supported baffled beam. They used an assumed-modes method to obtain frequency response functions of

the beam and the Rayleigh's integral to calculate the radiated sound power. A genetic-algorithm-based penalty function method was then employed to determine the optimal location, length, and shear modulus of the constrained-layer damping. However, their approach did not treat the temperature effect of damping layer and has limitations in extension to arbitrary complex geometry.

The complex modulus concept is widely used to describe the dynamic characteristic of viscoelastic damping materials [16]. The complex modulus of damping materials generally shows both frequency- and temperature-dependent storage modulus and a loss factor, which must be taken into account in the optimization formulation of a surface-layer damping design. Hence, objective and/or constraint functions should be frequency and temperature dependent. However, previous works that explored constrained-layer damping designs for noise problems used a constant assumption [13,14] or a simple exponential formula [15] that assumes frequency-dependent storage modulus but a constant loss factor. To consider frequency and temperature dependency of damping materials, the Golla–Hughes–McTavish model [17], the anelastic displacement field model [18], and the fractional–derivative model [12,19] can be used successfully in conjunction with the finite element method for damped structures. Among these models, the fractional–derivative model describes the dynamic properties of weak-frequency-dependent viscoelastic materials well using a small number of parameters over a broad frequency range, although its time domain analysis becomes more complicated. The author has proposed an optimization formulation for an unconstrained damping-layer layout for structural [12] and vibro-acoustic problems [20] using the equivalent stiffness and the iterative modal strain-energy method with real eigenvectors to calculate loss factors, which is justified by the relatively low damping of unconstrained-type damping. However, for constrained-type damping, the equivalent stiffness approach requires a complicated correction procedure and the damping is large. Thus, the errors due to an approximation of complex eigenvectors to real eigenvectors become larger than those in an unconstrained case. In this paper, previous works [12,20] are extended to constrained-type damping for structural-acoustic problems. The displacements of a constrained damping-layer beam are described layer by layer and are approximated by finite elements. The viscoelastic damping layer is modeled using the fraction derivative model to consider frequency- and temperature-dependent material properties. The resulting frequency-dependent complex eigenvalue problem is solved by an iterative scheme. Finally, a constrained damping-layer layout optimization formulation for interior noise problems is proposed with an analytic design sensitivity analysis. As numerical examples, the proposed method is applied to a constrained-layer damping beam radiating into a cavity to reduce interior noise by optimizing the damping-layer configuration.

II. Analysis of Vibro-Acoustic Systems

In this study, it is assumed that the structural-acoustic systems are semicoupled; that is, the structural responses influence the acoustic responses but the acoustic responses do not affect the vibration of the structures. As a result, vibro-acoustic problems can be solved sequentially. The structural problem should be solved first, and the velocity response of the structure is applied as the boundary condition of the acoustic problem.

A. Boundary-Element Analysis of Structural-Acoustic Problems

A boundary-element analysis for an acoustic cavity is one of the most common methods used, due to its accurate solution and simple preprocessing. Here, the direct boundary-element method is used to compute the interior sound pressure of an acoustic cavity, and a concise explanation is given.

A two-dimensional structural-acoustic problem for an isotropic and homogeneous medium with a closed boundary Γ, as shown in Fig. 1, is considered. The acoustic pressure of the time-harmonic waves in domain Ω satisfies the Helmholtz equation such that

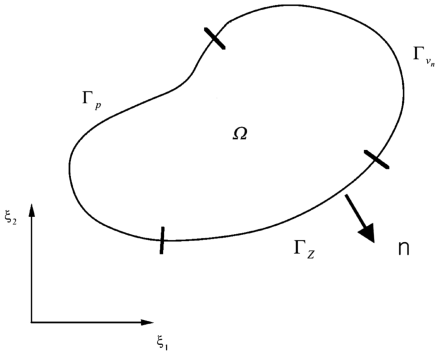

Fig. 1 Two-dimensional structural-acoustic problem.

$$\nabla^2 \boldsymbol{p}(\xi) + \kappa^2 \boldsymbol{p}(\xi) = 0 \tag{1}$$

where $\boldsymbol{p}(\xi)$ is the sound pressure and κ is the wave number. The sound pressure is subject to boundary conditions on boundary $\Gamma(=\Gamma_p \cup \Gamma_{v_n} \cup \Gamma_z)$, as follows:

$$\begin{aligned} &\boldsymbol{p}(\xi) = \boldsymbol{p}_0, \quad x \in \Gamma_p \qquad \boldsymbol{v}_n(\xi) \equiv -\frac{1}{i\omega\rho_0}\frac{\partial \boldsymbol{p}}{\partial n} = \boldsymbol{v}_{n0}, \quad x \in \Gamma_{v_n} \\ &\boldsymbol{z}(\xi) \equiv \boldsymbol{p}/\boldsymbol{v}_n = \boldsymbol{z}_0, \quad x \in \Gamma_z \end{aligned} \tag{2}$$

Here, ω, ρ_0, $\partial \boldsymbol{p}/\partial n$, and $\boldsymbol{v}_n$ are the angular velocity, the density, the normal component of pressure derivative, and the particle normal component of velocity, respectively. It is assumed that the velocity amplitude along the velocity boundary Γ_{v_n} is equal to the forced response of the structure, and that the influence of acoustic excitation on the structural response is negligible.

To obtain the sound pressure using the boundary-element method, the Helmholtz equation is transformed into an integral equation, and by discretizing the boundary integral, it becomes possible to obtain linear algebraic equations such as

$$\boldsymbol{AP} = \boldsymbol{BV}_n \tag{3}$$

where $\boldsymbol{A}$ and $\boldsymbol{B}$ are the system matrices, and $\boldsymbol{P}$ and $\boldsymbol{V}_n$ are the nodal sound pressure and normal velocity vectors, respectively. Applying the boundary conditions into the discretized equation, Eq. (3), the nodal sound pressures or normal velocities on the boundary can be calculated according to the boundary conditions. A detailed procedure of the boundary-element analysis is available in [21].

B. Analysis of Constrained-Layer Damping Beam

Constrained-layer damping attached on a structural wall is very effective in reducing structural vibration. Consider a partial constrained-layer damping patch on a base beam as shown in Fig. 2. Recently, although various finite element models [16,18,22,23] for sandwich beam structures have been developed, Sainsbury and Zhang [22] concluded through their comparative study that a 10-degree-of-freedom (DOF) beam element is preferred due to its high accuracy and low computing cost. Therefore, a 10-DOF beam element was chosen for the analysis of the constrained-layer damping beam. The 10-DOF beam element assumes that the base beam and the constraining layer satisfy the Bernoulli–Euler beam theory and undergo the same transverse and rotational deformations, and that the viscoelastic damping layer has an additional shear angle associated with nonnegligible transverse shear. Figure 3 shows the sign convention of the displacement field and the nodal degrees of freedom of the 10-DOF beam element. Considering the kinematic conditions of the displacements for the constrained-layer damping beam, and applying the virtual work principle and discretizing the resulting equation using the finite elements, it is possible to obtain the equations of motion, as

$$\boldsymbol{M}\ddot{\boldsymbol{x}} + \boldsymbol{Kx} = \boldsymbol{F} \tag{4}$$

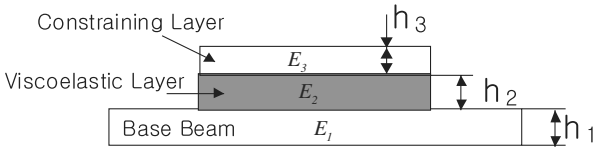

Fig. 2 Constrained viscoelastic damping-layer beam.

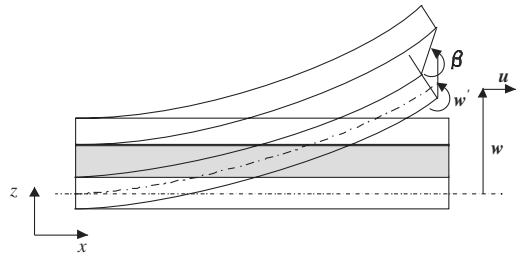

a) Displacements and sign conventions

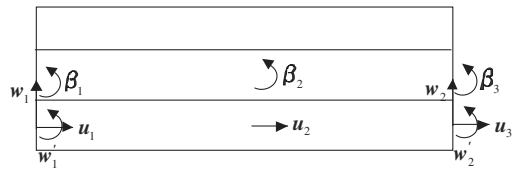

b) Nodal degrees of freedom of the beam element

Fig. 3 10-DOF finite element for constrained damping-layer beam.

Here, $\boldsymbol{M}$ and $\boldsymbol{K}$ represent the global mass and stiffness matrices, respectively, and $\boldsymbol{x}$ and $\boldsymbol{F}$ are the generalized displacement and force vectors, respectively. A detailed finite element formulation and the element stiffness and mass matrices expressions are found in [18]. At this point, it should be noted that the stiffness matrix $\boldsymbol{K}$ becomes a complex-valued matrix due to the viscoelastic damping layer. Assuming a harmonic motion of the system, the corresponding eigenvalue problem can be written as

$$\boldsymbol{K}\boldsymbol{y} = \lambda \boldsymbol{M}\boldsymbol{y} \tag{5}$$

where $\boldsymbol{y}$ is the complex eigenvector and λ is the complex eigenvalue. The ith eigenvector $\boldsymbol{y}_i$ satisfies the orthogonal conditions of the form

$$\boldsymbol{y}_i^T \boldsymbol{M}\boldsymbol{y}_j = \delta_{ij} m_j \tag{6}$$

$$\boldsymbol{y}_i^T \boldsymbol{K}\boldsymbol{y}_j = \delta_{ij} k_j \tag{7}$$

where δ_{ij} is the Kronecker delta and m_i and k_i are the generalized modal mass and the stiffness of the ith mode, respectively. To be unique eigenvectors, a normalization condition has to be introduced. However, the conventional normalization condition in a real symmetric system in which the magnitude of the eigenvector is set to one does not render the eigenvector unique [24]. In this study, the normalization condition that sets the mth component of the kth eigenvector y_k^m equal to one is imposed as follows:

$$y_k^m = 1 \tag{8}$$

This guarantees the uniqueness of the eigenvector. The index m can be selected from the maximum component of the kth eigenvector, as

$$|y_k^m| = \max_j |y_k^j| \tag{9}$$

As Murthy and Haftka [24] stated, this normalization condition is very attractive because it avoids the ill conditioning of the system matrix in the design sensitivity calculation step.

The natural frequency μ_k and the modal loss factor η_k of the kth mode are defined as

$$\mu_k = \frac{\sqrt{\mathrm{Re}(\lambda_k)}}{2\pi}, \qquad \eta_k = \frac{\mathrm{Im}(\lambda_k)}{\mathrm{Re}(\lambda_k)} \tag{10}$$

where Re and Im refer to the real and the imaginary parts of the argument, respectively.

The dynamic characteristics of viscoelastic materials used for constrained-layer damping vary with the temperature as well as the frequency. Hence, the variation of the complex modulus has to be included in the finite element formulation. First, from the temperature-frequency superposition principle of viscoelastic materials [25], knowing the complex modulus of a viscoelastic material over the entire frequency range at a reference temperature, the shift factor $\alpha(T)$ enables the prediction of the complex modulus at any temperatures. The shift factor transforms temperature effects in the complex modulus into the frequency shift and is related to temperature through the Arrhenius equation [26], as in

$$\log[\alpha(T)] = d_1\left(\frac{1}{T} - \frac{1}{T_0}\right) \tag{11}$$

where d_1 is a constant and T_0 is the reference temperature in absolute degrees.

Next, considering the variation of the complex modulus of viscoelastic materials in the frequency domain, it is known that the four-parameter fractional–derivative model is sufficient to represent the real behavior of viscoelastic materials over a wide frequency range [19]. The complex modulus represented by the fractional–derivative model in the frequency domain can be written as follows [12,26]:

$$\boldsymbol{E} = \frac{a_0 + a_1[\boldsymbol{i}f\alpha(T)]^\beta}{1 + c_1[\boldsymbol{i}f\alpha(T)]^\beta} \tag{12}$$

Here, the four material parameters a_0, a_1, c_1, and β in Eq. (12) must be identified in a suitable empirical manner. Figure 4 shows a typical example of a complex modulus variation of a damping material ISD-110 represented by the fractional–derivative model [26].

The fractional–derivative model used in this paper to describe the dynamic characteristics of the viscoelastic damping layer makes the stiffness matrix frequency dependent. Therefore, the eigenvalue problem of Eq. (5) also becomes frequency dependent. To solve the frequency-dependent eigenvalue problem, it is necessary to introduce an iterative scheme, such as the Newton–Raphson method [27]. In this study, a simple resubstitution method [12] is used to solve the frequency-dependent complex eigenvalue problem. The iterative procedure is summarized well in [28].

To calculate the forced responses of the constrained-layer damping beam, the modal superposition method is used. The velocity of the structure due to a harmonic force of magnitude $\boldsymbol{F}$ with angular velocity ω can then be written as

$$\boldsymbol{v} = \sum_{k=1}^{N_m} \boldsymbol{i}\omega a_k \boldsymbol{y}_k \tag{13}$$

where N_m is the number of the mode and a_k the kth modal coordinate, as follows:

$$a_k = \frac{\boldsymbol{y}_k^T \boldsymbol{F}}{(\lambda_k - \omega^2) m_k} \tag{14}$$

Calculating the velocity response of the structures using Eq. (13), the velocity is transformed into the normal component to the structure and plugged into the boundary-element equation, Eq. (3), to obtain the acoustic responses.

C. Numerical Examples

To calculate the responses of the constrained beam structure, the 10-DOF finite element code of the previous section is developed. Numerical examples are introduced to check the validity of the proposed method. The first example is a cantilever beam fully

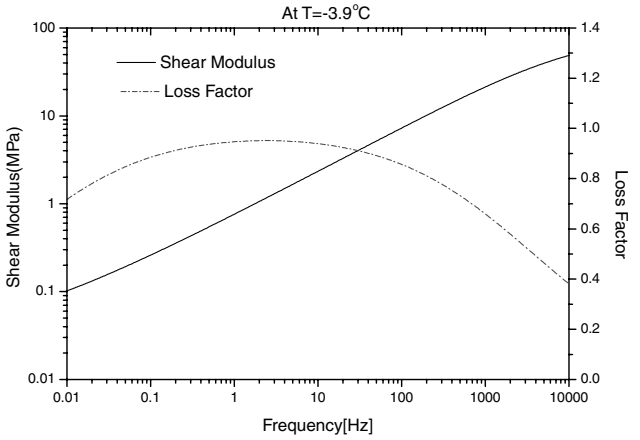

a) Frequency variation

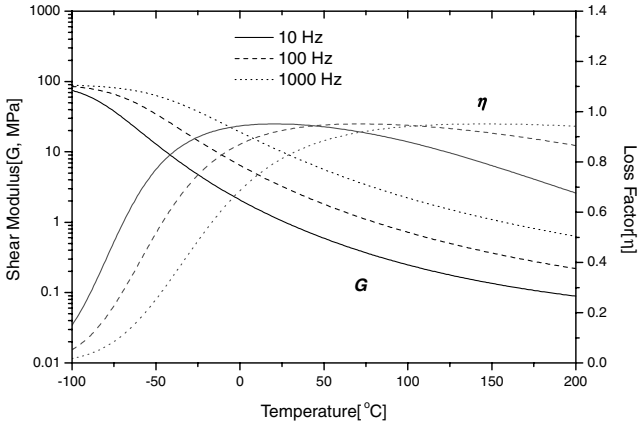

b) Temperature variation

Fig. 4 Example of complex modulus variation of a material (ISD-110).

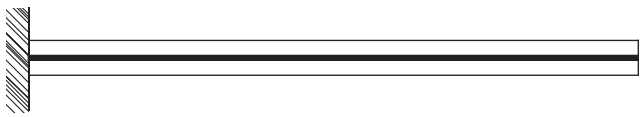

Fig. 5 Cantilever sandwich beam problem.

covered by a constrained-layer damping, as shown in Fig. 5. The material properties and beam dimensions are listed in Table 1. The length and width of the beam are 177.8 and 12.7 mm, respectively. The complex modulus of the viscoelastic damping material in the example is assumed to be constant, and its loss factor is denoted as η_c. The constrained-layer damping beam is discretized by 20 elements and assembled to form the global stiffness and mass matrices. With various values of η_c, the complex eigenvalue problems are solved using the International Mathematical and Statistical Library routine *dgvccg*, which uses the QZ algorithm [29]. From the computed eigenvalues, the natural frequencies and the loss factors of each mode are calculated using Eq. (10). In Table 2, the results are listed and compared with the analytical results from Daya and Potier-Ferry [27]. Table 2 shows that the present method can accurately predict

Table 1 Material properties of the beam problem

	Elastic layers	Viscoelastic layer
Young's modulus, N/m^2	6.9E + 10	1.794E + 6
Poisson's ratio	0.3	0.3
Density, kg/m^3	2766	968.1
Thickness, mm	1.524	0.127

eigenfrequencies and loss factors of constrained-layer damping beam structures. It is also accurate for high damping.

Next, to validate the analysis procedure of structural-acoustic problems, a numerical example is introduced. This is shown in Fig. 6. In the example, a rectangular cavity is surrounded by rigid walls excluding the bottom side. A pinned–pinned aluminum beam closes the cavity, and the viscoelastic damping material ISD-110 is used with a constraining aluminum layer. A unit force F is imposed on the center of the aluminum beam. The thicknesses of the base beam, the damping layer, and the constraining layer are 20, 2, and 2 mm, respectively. The parameters of the fractional–derivative model and the shift factor of ISD-110 are available in [26]. For the modeling of the cavity, an in-house boundary-element code that uses quadratic shape functions was developed; previous work by the author [20] showed the validity of the developed code by comparing its results with those of a commercial software program. For this reason, the comparison is not reiterated here. Instead, a numerical procedure that explains the computation of the vibro-acoustic responses is given. The constrained-layer damping beam of the example is discretized with 20 elements using the 10-DOF finite elements for the constrained part and the degenerated elements for the bared part. Following this, a resubstitution method solves the frequency-dependent complex eigenproblem by repeating the solution procedure of the constant complex eigenvalue problem until the eigenvalues converge. Typically, the iterations end after the constant complex eigenvalue problem is solved three or four times. From the calculated eigenvalues and eigenvectors, the modal superposition method gives the structural responses of the constrained-layer damping beam in the form of velocity, which is plugged into the normal velocity boundary condition of the cavity problem. The boundary of the cavity is modeled with equally spaced 40 quadratic boundary elements. For a case involving half coverage of the constrained part ($L = 250$ mm), the sound pressure level at point A is calculated using the proposed method. The frequency band was from 20–1000 Hz with 1 Hz increments. Figure 7 shows calculation results in which two cases are plotted. In the first case, the three walls are treated as rigid walls. In the second case, a heavy sound-absorption material covers the three walls; in this case the impedance value of the walls is $1/0.7(1\text{-}i)$ times the characteristic impedance of air. As shown in Fig. 7, many sharp peaks exist in the example with rigid wall as a result of cavity resonances. Also shown in Fig. 7 is that the cavity resonance peaks disappear after coverage with sound-absorption material. However, as shown in Fig. 7 the structure-induced peaks could not be suppressed by absorption materials because the structural vibration acts as a sound source. Therefore, to control the structure-induced peaks, the structural vibration must be reduced by active or passive damping treatments.

Table 2 Natural frequencies and loss factors of the sandwich beam problem

	Analytic method		Present method			
η_c	μ_m	η_m/η_c	μ_m		η_m/η_c	
	Hz	——	Hz	Error (%)	——	Error, %
0.1	64.1	0.282	64.1	0.04	0.281	−0.19
	296.4	0.242	296.6	0.08	0.242	0.13
	743.7	0.154	744.2	0.07	0.154	0.09
	1393.9	0.089	1394.7	0.05	0.089	−0.09
0.6	64.5	0.246	65.5	0.06	0.246	0.00
	298.9	0.232	299.1	0.08	0.232	0.09
	745.5	0.153	746.0	0.06	0.153	−0.19
	1394.9	0.089	1395.6	0.05	0.089	−0.44
1.5	69.9	0.153	69.9	0.05	0.153	0.04
	308.9	0.197	309.1	0.06	0.197	0.23
	754.0	0.146	755.0	0.13	0.146	−0.01
	1399.7	0.087	1400.4	0.05	0.087	0.36

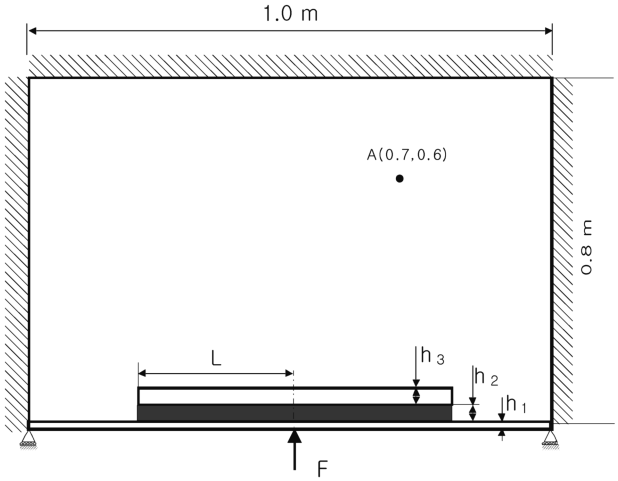

Fig. 6 Rectangular cavity problem enclosed with a pinned–pinned beam.

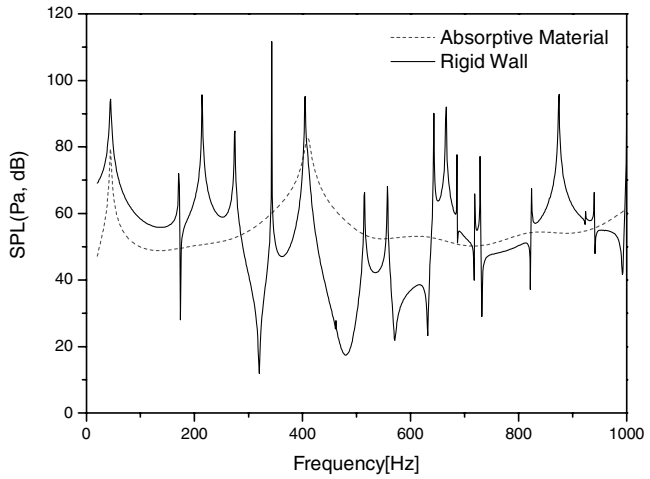

Fig. 7 Calculated interior sound pressure levels at point A.

III. Design Sensitivity Analysis

The amount of noise reduction by constrained-layer damping is dependent upon the design parameters, including the location of the damping patch, the thicknesses of the damping and constraining layers, and the properties of the damping material. To determine the optimal damping-layer layout, the influence of each design parameter on a concerned function should initially be obtained quantitatively. It is then possible to obtain the optimum layout for constrained-layer damping using a gradient-based mathematical programming algorithm. The quantitative rate of change of a function with respect to a design change is the design sensitivity. The objective or constraint functions in an optimal damping-layer layout design problem are a function of the interior sound pressure level; thus, a structural-acoustic design sensitivity analysis is needed. Many researchers have proposed design sensitivity formulations for vibro-acoustic problems using the boundary-element method [30,31], finite element method [32,33], or a hybrid method [34]. In this study, a direct differentiation method is applied to the discrete system equations to obtain a design sensitivity formula with respect to the design parameters for an acoustic response.

The direct differentiation of a boundary equation for an interior point yields the design sensitivity formula for an interior acoustic response. Similar to the acoustic response calculation, the resulting sound pressure sensitivity must be postprocessed from the design sensitivities of the sound pressure and the normal component of boundary velocity. To obtain the design sensitivities on the boundary, the discretized boundary-element equation can be differentiated with respect to the design variables. The relationship between the sound pressure sensitivity vector and the normal velocity sensitivity vector on the boundary can then be obtained, as follows:

$$\boldsymbol{A}\frac{\partial \boldsymbol{P}}{\partial \boldsymbol{b}} = \boldsymbol{B}\frac{\partial \boldsymbol{V}_n}{\partial \boldsymbol{b}} \tag{15}$$

where $\boldsymbol{b}$ is the design parameter. Here, $\partial \boldsymbol{P}/\partial \boldsymbol{b}$ and $\partial \boldsymbol{V}_n/\partial \boldsymbol{b}$ are the design sensitivity vectors of the sound pressure and normal velocity, respectively, of which the components are values on each boundary node. Equation (15) is similar to Eq. (3), apart from the boundary conditions, implying that the cost of the design sensitivity computation is very low. Examining Eq. (15), the design sensitivity for sound pressure on the boundary can be calculated if the normal velocity sensitivity vector on the boundary is known. The design sensitivity expression of the normal velocity on the boundary can be derived from the forced response expression of the structure, Eq. (13), by differentiation with respect to the design parameter, as follows:

$$\frac{\partial \boldsymbol{v}}{\partial \boldsymbol{b}} = i\omega \sum_{k=1}^{N_m} \left\{ \frac{\partial a_k}{\partial \boldsymbol{b}} \boldsymbol{y}_k + a_k \frac{\partial \boldsymbol{y}_k}{\partial \boldsymbol{b}} \right\} \tag{16}$$

where

$$\frac{\partial a_k}{\partial \boldsymbol{b}} = \frac{\partial \boldsymbol{y}_k^T}{\partial \boldsymbol{b}} \boldsymbol{F} \times [(\lambda_k - \omega^2) m_k]^{-1} - \frac{\boldsymbol{y}_k^T \boldsymbol{F} [\frac{\partial \lambda_k}{\partial \boldsymbol{b}} m_k + i(\lambda_k - \omega^2) \cdot \frac{\partial m_k}{\partial \boldsymbol{b}}]}{[(\lambda_k - \omega^2) m_k]^2} \tag{17}$$

Here it is noted that the normal velocity sensitivity expression consists of eigenvectors, eigenvalues, and generalized modal mass sensitivities.

First, differentiating the orthogonal condition of eigenvectors, Eq. (6), with respect to the design variable and applying the symmetric property of the mass matrix, the generalized modal mass sensitivity can be obtained as follows:

$$\frac{\partial m_k}{\partial \boldsymbol{b}} = 2\frac{\partial \boldsymbol{y}_k^T}{\partial \boldsymbol{b}} \boldsymbol{M} \boldsymbol{y}_k + \boldsymbol{y}_k^T \frac{\partial \boldsymbol{M}}{\partial \boldsymbol{b}} \boldsymbol{y}_k \tag{18}$$

It is noted that $\partial \boldsymbol{M}/\partial \boldsymbol{b}$ can be calculated analytically from the mass matrix expression of the finite element formulation. Therefore, the only additional unknown in the calculation of the generalized modal mass sensitivity is the eigenvector sensitivities of each mode.

Next, the eigenvalue sensitivity formula for the kth eigenvalue, $\partial \lambda_k/\partial \boldsymbol{b}$, in a discrete form, is also obtained by differentiating the complex eigenvalue problem equation for the kth eigenvalue and eigenvector. Premultiplying the kth eigenvector with the resulting equation and applying the orthogonal condition, the eigenvalue sensitivity formula can be obtained by the following equation:

$$\frac{\partial \lambda_k}{\partial \boldsymbol{b}} = \frac{1}{m_k} \cdot \left(\boldsymbol{y}_k^T \frac{\partial \boldsymbol{K}}{\partial \boldsymbol{b}} \boldsymbol{y}_k - \lambda_k \boldsymbol{y}_k^T \frac{\partial \boldsymbol{M}}{\partial \boldsymbol{b}} \boldsymbol{y}_k \right) \tag{19}$$

Similar to the mass matrix case, the stiffness matrix expression in the finite element formulation gives analytical expressions of $\partial \boldsymbol{K}/\partial \boldsymbol{b}$.

Finally, the last unknown related to the interior sound pressure sensitivity is the complex eigenvector sensitivity formula. Eigenvector sensitivity formulations for real eigenvalue problems have been developed by many researchers and are fairly well established at present [35–37]. However, the formulations for real-valued problems can not be applied to a complex eigenvalue problem as the normalization condition for complex eigenvectors is quite different for a complex eigenvalue problem. Murthy and Haftka [24] proposed an efficient eigenvector sensitivity formulation for a general complex eigenvalue problem. Following Murthy and Haftka's formulation, the complex eigenvector sensitivity formulation is explained briefly for the constrained-layer damping beam problem.

The kth eigenvector, $\boldsymbol{y}_k$, satisfies the following equation:

$$\boldsymbol{K}\,\boldsymbol{y}_k = \lambda_k \boldsymbol{M}\boldsymbol{y}_k \tag{20}$$

Differentiating the aforementioned equation with respect to the design variable, the following equation can be obtained:

$$(\boldsymbol{K} - \lambda_k \boldsymbol{M})\frac{\partial \boldsymbol{y}_k}{\partial \boldsymbol{b}} - (\boldsymbol{M}\boldsymbol{y}_k)\frac{\partial \lambda_k}{\partial \boldsymbol{b}} = -\left[\frac{\partial \boldsymbol{K}}{\partial \boldsymbol{b}} - \lambda_k \frac{\partial \boldsymbol{M}}{\partial \boldsymbol{b}}\right]\boldsymbol{y}_k \tag{21}$$

At this point, Eq. (21) can be rewritten in partitioned matrix form:

$$[\,\boldsymbol{K} - \lambda_k \boldsymbol{M} \quad |\boldsymbol{M}\boldsymbol{y}_k\,]\begin{Bmatrix} \frac{\partial \boldsymbol{y}_k}{\partial \boldsymbol{b}} \\ \frac{\partial \lambda_k}{\partial \boldsymbol{b}} \end{Bmatrix} = -\left[\frac{\partial \boldsymbol{K}}{\partial \boldsymbol{b}} - \lambda_k \frac{\partial \boldsymbol{M}}{\partial \boldsymbol{b}}\right]\boldsymbol{y}_k \tag{22}$$

Equation (22) is a system of n equations with $n + 1$ unknown, in which n represents the total degrees of freedom of the system. Consequently, the system matrix of Eq. (22) has a rank deficiency of 1. However, differentiating the normalization condition of eigenvectors, as in Eq. (8), one component of the unknown vector is known:

$$\frac{\partial y_k^m}{\partial \boldsymbol{b}} = 0 \tag{23}$$

Plugging Eq. (23) into Eq. (22), the mth column of the coefficient matrix is eliminated and the number of unknowns reduced by one, so that the resulting equations become a system of n equations with n unknowns, as follows:

$$\boldsymbol{C}\boldsymbol{q} = \boldsymbol{r} \tag{24}$$

where

$$\begin{aligned} \boldsymbol{C} &= [\,\boldsymbol{K} - \lambda_k \boldsymbol{M} \quad |\boldsymbol{M}\boldsymbol{y}_k\,]_{m\text{th column deleted}} \\ \boldsymbol{q} &= \left\{ \frac{\partial y_k^1}{\partial \boldsymbol{b}} \quad \cdots \quad \frac{\partial y_k^{m-1}}{\partial \boldsymbol{b}} \quad \frac{\partial y_k^{m+1}}{\partial \boldsymbol{b}} \quad \cdots \quad \frac{\partial y_k^n}{\partial \boldsymbol{b}} \quad \frac{\partial \lambda_k}{\partial \boldsymbol{b}} \right\}^T \\ \boldsymbol{r} &= -\left[\frac{\partial \boldsymbol{K}}{\partial \boldsymbol{b}} - \lambda_k \frac{\partial \boldsymbol{M}}{\partial \boldsymbol{b}}\right]\boldsymbol{y}_k \end{aligned} \tag{25}$$

Given that the matrix $\boldsymbol{C}$ is nonsingular [24], the eigenvector and eigenvalue sensitivities can be obtained simultaneously using a standard linear solver. Here, it is interesting that the eigenvalue sensitivity can be computed from either Eq. (19) or Eq. (24), as needed.

In summary, to obtain the design sensitivity information for an interior sound pressure response, it is necessary to solve one eigenvalue problem, one eigenvalue sensitivity analysis, and one eigenvector sensitivity analysis on the structural side. On the acoustic side, one additional linear algebraic equation, represented by Eq. (15), and several manipulations of matrices and vectors are needed to calculate the sensitivity information. However, it should be noted that the system matrices of the acoustic design sensitivity calculation in Eq. (15) are the same matrices as those for the sound pressure calculation. Therefore, the additional cost of the design sensitivity analysis of the interior sound pressure is not high, as it requires only a small number of algebraic calculations for the additional load vectors.

To validate the proposed design sensitivity analysis procedure numerically, an example identical to the previous section is introduced, as shown in Fig. 6. The length of the damping layer L and the thicknesses of the damping and constraining layers are selected as the design variables. The base beam thickness is fixed at 20 mm. The design sensitivities of the interior sound pressure at point A are calculated and compared with those of the forward finite difference method (FDM) as

$$\frac{d\boldsymbol{p}}{d\boldsymbol{b}} \cong \frac{\Delta \boldsymbol{p}}{\Delta \boldsymbol{b}} = \frac{\boldsymbol{p}(\boldsymbol{b} + \Delta \boldsymbol{b}) - p(\boldsymbol{b})}{\Delta \boldsymbol{b}} \tag{26}$$

where $\Delta \boldsymbol{b}$ is the amount of the perturbation of the design variable. For the finite difference method, a perturbation of 0.1% of the design variable is used. Figure 8 shows the sensitivity results compared with those of the FDM. The two results are in good agreement, which proves that the proposed design sensitivity formulation and the numerical implementations are correct. It should also be noted that the proposed design sensitivity formulation has advantages in terms of accuracy and computational speed, whereas the finite difference method is simple and straightforward in implementation. In Table 3, computational times for the sensitivity analysis in the rectangular cavity problem are compared. As shown in Table 3, the proposed sensitivity analysis method is very efficient and only a little additional time compared with that of the response analysis is sufficient to obtain sensitivity information.

IV. Optimization of Constrained-Layer Damping Layout

The goal of a damping treatment on structures in structural-acoustic systems is to minimize the vibrations or sound power radiated from the structure. At the same time, the added weight by constrained-layer damping should be minimized as it increases manufacturing or/and operational costs. However, these two goals generally move in opposite directions when a design parameter changes. In this situation, an optimization technique could be a solution in the determination of a trade-off point in the design of a constrained-layer damping layout. A gradient-based method is adopted for the optimization of the constrained-layer damping design in this study, as the gradient-based method is on average among the most efficient methods in this area of engineering even though it may yield a local minimum. In addition, one objective function is assumed, so that one goal is selected as an objective function and the other is treated as a constraint.

Assuming uniformly coated constrained-layer damping, the optimal design problem of the damping treatment layout in structural-acoustic problems can be defined as follows:

$$\begin{aligned} &\text{Find } \boldsymbol{b} = \{\, L \quad h_2 \quad h_3 \,\}^T \\ &\quad \text{such that minimize} \quad \text{weight } (\boldsymbol{b}) \\ &\quad \text{subject to} \quad g[\boldsymbol{p}(f, T), \boldsymbol{b}] \le 0 \\ &\quad \text{and} \quad \boldsymbol{b}_L \le \boldsymbol{b} \le \boldsymbol{b}_U \end{aligned} \tag{27}$$

where $\boldsymbol{b}$ is the design variable vector and $\boldsymbol{b}_L$ and $\boldsymbol{b}_U$ are the lower and upper bounds of the design variables, respectively. The objective function is the weight added by the constrained-layer damping, which can be written as

$$\text{weight} = 2L(\rho_2 h_2 + \rho_3 h_3) \tag{28}$$

In Eq. (28), a symmetric treatment of the constrained-layer damping is assumed for brevity. The constraint function g is a target level of sound pressure responses. In this study, the constraint function g is of the form

$$g = \int_{f_1}^{f_2} \langle 20 \log(\|\boldsymbol{p}\|/p_{\text{ref}}) - p_{\text{dB0}} \rangle \, \mathrm{d}f \tag{29}$$

where

$$\langle x \rangle = \begin{cases} x & \text{if } x > 0 \\ 0 & \text{if } x \le 0 \end{cases} \tag{30}$$

Here, $P_{\text{ref}} = 20 \times E - 6$ and p_{dB0} is a target level represented in decibel scale. Using mathematical programming techniques, it is then possible to find the solution of the optimization problem defined by Eq. (27). In this study, the optimization software IDESIGN [38] was used to solve the optimization problem. The gradient information of the constraint function was computed using the proposed method and plugged into the optimization software.

According to the optimization formulation proposed in Eq. (27), the optimal constrained-layer damping designs are identified for the same example shown in Fig. 6. The dimension of the base beam is also fixed as $h_1 = 20$ mm. As shown in Fig. 7, two peaks are present in the acoustic response at point A, which are induced by the first and third structural resonance modes. Hence, the optimal constrained-

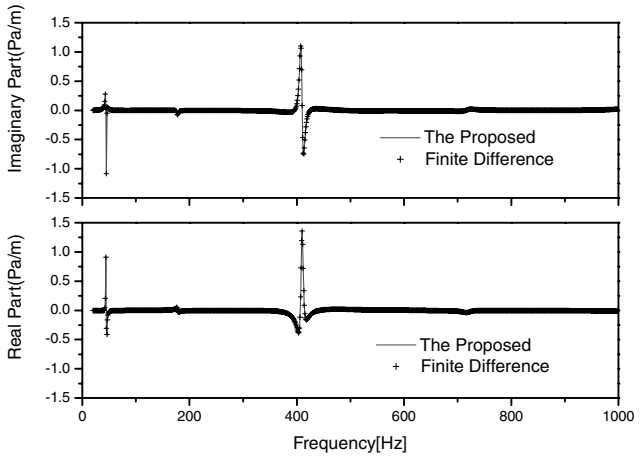

a) For L

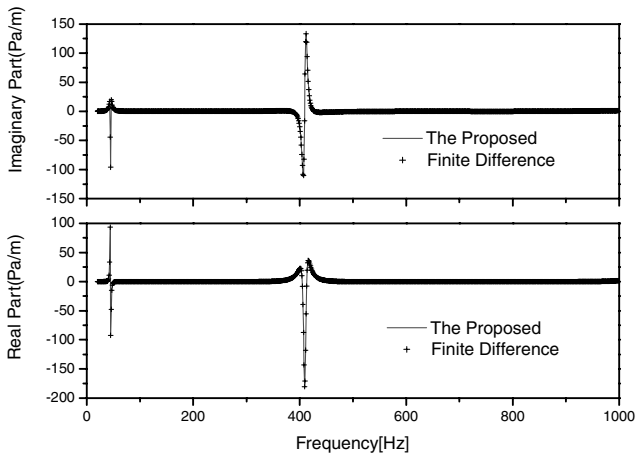

b) For h_2

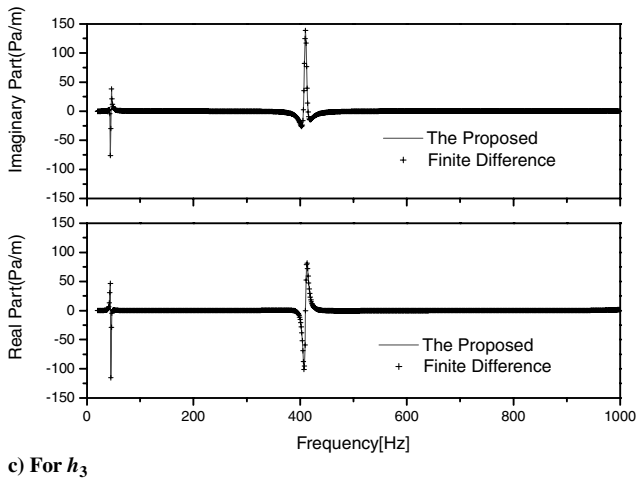

c) For h_3

Fig. 8 Sound pressure sensitivities of the rectangular cavity problem compared with those of the FDM.

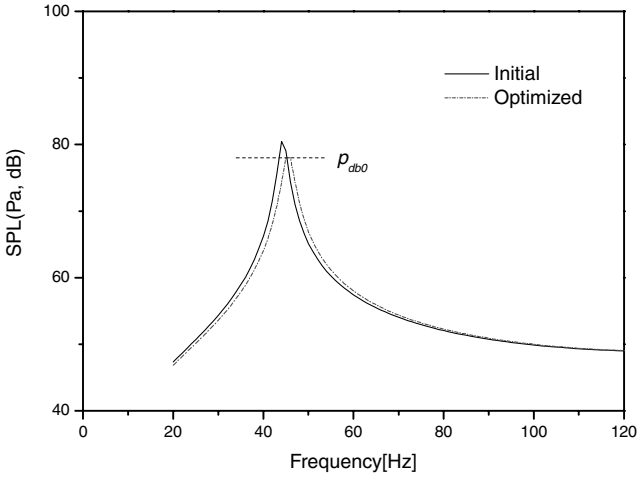

a) $T=30\,^{\circ}C$

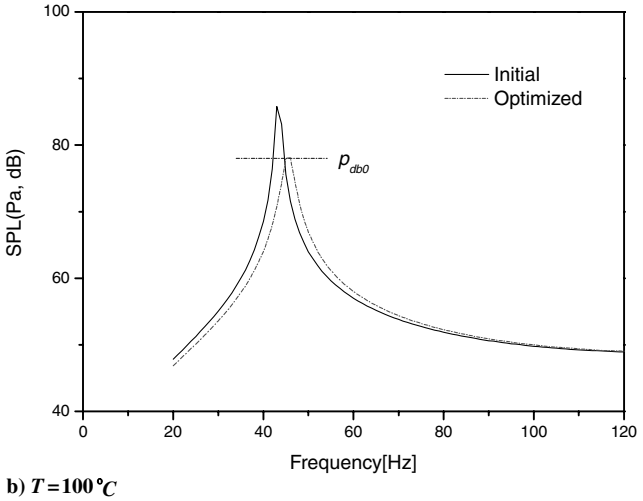

b) $T=100\,^{\circ}C$

Fig. 9 Sound pressure levels at the initial and optimal damping layouts for case 1.

layer damping designs are found for two cases. The first case (case 1) includes only the first peak in the calculation of the constraint function, Eq. (29), by selecting frequency range around the peak. The second case (case 2) includes both peaks. Additionally, two temperatures of 30 and 100°C were selected to investigate temperature effects. To prevent mesh distortion on the structure boundary during iterations, the nodes of the beam mesh were moved proportional to the design variables. Table 4 shows the function parameters and the optimization results. In Figs. 9 and 10, the sound pressure levels at the optimal damping layouts are compared to those at the initial damping layouts. As listed in Table 4, the optimal layouts of the constrained-layer damping are dependent upon the temperatures. For case 1, the thickness of the constraining layer became thicker, whereas the thickness of the damping layer became thinner. However, the length of the constrained-layer damping showed little change from the initial value, as the order of magnitude

Table 3 Comparison of computational times for the sound pressure level sensitivity analysis of the rectangular cavity problem

		CPU time[a], s	Ratio to A, %
Response analysis		211 (A)	100
Sensitivity analysis	Proposed method	17	8.06
	FDM	633	300

[a]WIN2000 1.0 GHz Pentium4 PC with 512 Mb RAM was used.

Table 4 Optimization results for the rectangular cavity problem

		Optimum values			
	Initial values	Case 1: first peak		Case 2: all peaks	
T, °C	——	30	100	30	100
p_{dB0}, dB	——	78	78	78	78
L, mm	250	249.4	250.0	204.4	201.5
h_2, mm	2	0.804	0.187	0.678	0.143
h_3, mm	2	2.268	2.494	3.629	3.736
Weight, %	100	94.25	94.82	117.08	113.02

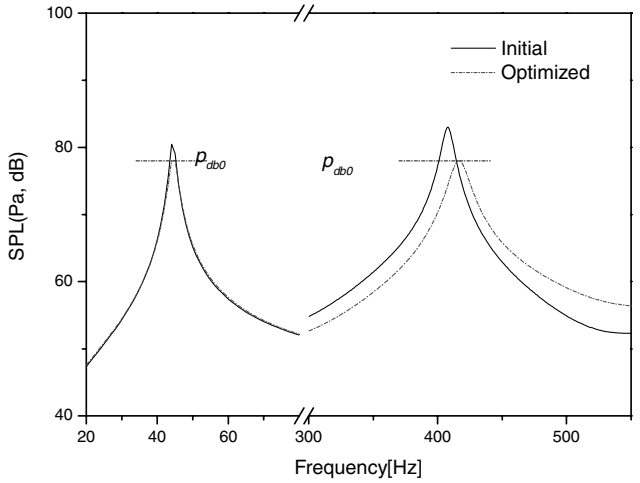

a) T = 30 °C

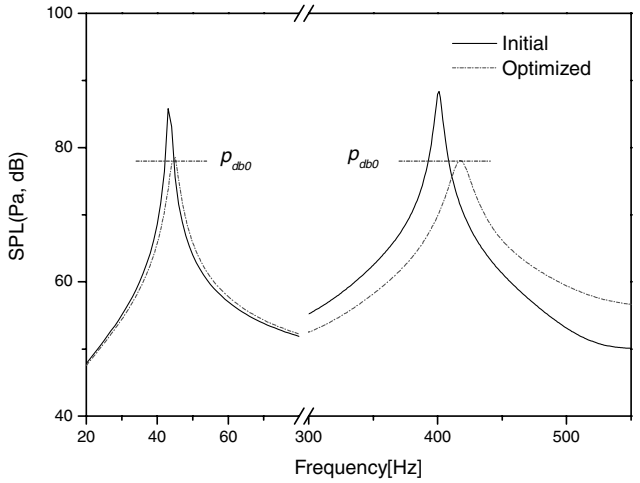

b) T = 100 °C

Fig. 10 Sound pressure levels at the initial and optimal damping layouts for case 2.

of the length sensitivity is 2 or 3 orders smaller compared to that of the thickness sensitivities, as expected from Fig. 8. Thus, it can be concluded that the length of the constrained-layer damping is not the first choice; instead, the thicknesses of the layers is, if the constrained-layer damping layout is modified for the purpose of interior noise reduction. For case 2, within the initially given weight, a damping-layer layout that satisfies the interior noise constraint was not found; consequently, the weight increased as much as the constraint function would allow. Also shown in Figs. 9 and 10 is that the proposed optimization formulation can effectively lower the interior noise level to the limit by changing the layout of the constrained-layer damping.

V. Conclusions

An optimization method to determine the optimal layout of constrained-layer damping on a structure is proposed using a gradient-based numerical search algorithm for structural-acoustic problems. It has shown that the proposed method can successfully describe the frequency- and temperature-dependent dynamic characteristics of a constrained-layer damping beam, even for high damping, by introducing the fractional–derivative model of viscoelastic materials and by solving the complex eigenvalue problem. In addition, this research has demonstrated that the finite element/boundary-element mixed approach can accurately predict the effect of the damping layer on interior sound pressure level. It has also shown that the proposed sensitivity formulation of acoustic noise is not only efficient but also accurate. The sensitivity analysis results show that thickness change of constrained-layer damping will be more effective than length change when one controls interior noise. The results of the numerical example show that the optimal damping layout is highly dependent upon the temperature, and that the proposed method can identify the optimal damping-layer layout effectively.

Acknowledgment

This work was supported by a Korea Science and Engineering Foundation (KOSEF) grant funded by the Korean government (MOST) (grant no. R01-2007-000-10986-0).

References

[1] Mead, D. J., *Passive Vibration Control*, Wiley, New York, 2000.

[2] Rao, M. D., "Recent Applications of Viscoelastic Damping for Noise Control in Automobiles and Commercial Airplanes," *Journal of Sound and Vibration*, Vol. 262, 2003, pp. 457–474. doi:10.1016/S0022-460X(03)00106-8

[3] Kruger, D. H., and Mann, J. A., III, "Minimizing the Sound Power Radiated by a Cube as a Function of the Size of Constrained Layer Damping Patches," *Journal of the Acoustical Society of America*, Vol. 105, No. 3, 1999, pp. 1714–1724. doi:10.1121/1.426701

[4] Plunkett, R., and Lee, C. T., "Length Optimization for Constrained Viscoelastic Layer Damping," *Journal of the Acoustical Society of America*, Vol. 48, No. 1, 1970, pp. 150–161. doi:10.1121/1.1912112

[5] Lall, A. K., Nakra, B. C., and Asnani, N. T., "Optimum Design of Viscoelastically Damped Sandwich Panels," *Engineering Optimization*, Vol. 6, 1983, pp. 197–205. doi:10.1080/03052158308902470

[6] Lifshitz, J. M., and Leibowitz, M., "Optimal Sandwich Beam Design for Maximum Viscoelastic Damping," *International Journal of Solids and Structures*, Vol. 23, No. 7, 1987, pp. 1027–1034. doi:10.1016/0020-7683(87)90094-1

[7] Marcelin, J. L., Trompette, P., and Smatic, A., "Optimal Constrained Layer Damping with Partial Coverage," *Finite Elements in Analysis and Design*, Vol. 12, 1992, pp. 273–280. doi:10.1016/0168-874X(92)90037-D

[8] Baz, A., and Ro, J., "Optimum Design and Control of Active Constrained Layer Damping," *Journal of Mechanical Design*, Vol. 117, June 1995, pp. 135–144, Special Issue.

[9] Nakra, B. C., "Vibration Control in Machines and Structures Using Viscoelastic Damping," *Journal of Sound and Vibration*, Vol. 211, No. 3, 1998, pp. 449–465. doi:10.1006/jsvi.1997.1317

[10] Zheng, H., Cai, C., and Tan, X. M., "Optimization of Partial Constrained Layer Damping Treatment for Vibrational Energy Minimization of Vibrating Beams," *Computers and Structures*, Vol. 82, 2004, pp. 2493–2507. doi:10.1016/j.compstruc.2004.07.002

[11] Kim, T. W., and Kim, J. H., "Eigensensitivity Based Optimal Distribution of a Viscoelastic Damping Layer for a Flexible Beam," *Journal of Sound and Vibration*, Vol. 273, 2004, pp. 201–218. doi:10.1016/S0022-460X(03)00479-6

[12] Lee, D. H., and Hwang, W. S., "Layout Optimization of Unconstrained Viscoelastic Layer on Beams Using Fractional Derivative Model," *AIAA Journal*, Vol. 42, No. 10, 2004, pp. 2167–2170.

[13] Azzouz, M. S., and Ro, J., "Control of Sound Radiation of an Active Constrained Layer Damping Plate/Cavity System Using the Structural Intensity Approach," *Journal of Vibration and Control*, Vol. 8, No. 6, 2002, pp. 903–918. doi: 10.1177/1077546029307

[14] Gibbs, G. P., and Cabell, R. H., "Active/Passive Control of Sound Radiation from Panels Using Constrained Layer Damping," AIAA Paper 2003-1813, 2003.

[15] Zheng, H., and Cai, C., "Minimization of Sound Radiation from Baffled Beams Through Optimization of Partial Constrained Layer Damping Treatment," *Applied Acoustics*, Vol. 65, 2004, pp. 501–520. doi:10.1016/j.apacoust.2003.11.008

[16] Trindade, M. A., and Benjeddou, A., "Hybrid Active-Passive Damping Treatments Using Viscoelastic and Piezoelectric Materials: Review and Assessment," *Journal of Vibration and Control*, Vol. 8, No. 6, 2002, pp. 699–745. doi: 10.1177/1077546029186

[17] Trindade, M. A., Benjeddou, A., and Ohayon, R., "Finite Element

Analysis of Frequency- and Temperature-Dependent Hybrid Active-Passive Vibration Damping," *Revue Européenne des Eléments Finis*, Vol. 9, Nos. 1-2-3, 2000, pp. 89–111.

[18] Lesieutre, G. A., and Lee, U., "A Finite Element for Beams Having Segmented Active Constrained Layers with Frequency-Dependent Viscoelastics," *Smart Materials and Structures*, Vol. 5, 1996, pp. 615–627. doi:10.1088/0964-1726/5/5/010

[19] Torvik, P. J., and Bagley, R. L., "On the Appearance of the Fractional Derivative in the Behavior of Real Material," *Journal of Applied Mechanics*, Vol. 51, 1984, pp. 294–298.

[20] Lee, D. H., "Minimization of Sound Pressure Levels in Vibro-Acoustic Systems Using Optimal Distribution of a Viscoelastic Damping Layer," *CD–ROM Proceedings of 6th World Congress on Structural and Multidisciplinary Optimization*, International Society for Structural and Multidisciplinary Optimization, Brazil, 2005.

[21] Wu, T. W. (ed.), *Boundary Element Acoustics: Fundamentals and Computer Codes*, WIT Press, Ashurst, U.K., 2000.

[22] Sainsbury, M. G., and Zhang, Q. J., "The Galerkin Element Method Applied to the Vibration of Damped Sandwich Beams," *Computers and Structures*, Vol. 71, 1999, pp. 239–256. doi:10.1016/S0045-7949(98)00242-9

[23] Teng, T. L., and Hu, N. K., "Analysis of Damping Characteristics for Viscoelastic Laminated Beams," *Computer Methods in Applied Mechanics and Engineering*, Vol. 190, 2001, pp. 3881–3892.

[24] Murthy, D. V., and Haftka, R. T., "Derivatives of Eigenvalues and Eigenvectors of a General Complex Matrix," *International Journal for Numerical Methods in Engineering*, Vol. 26, 1988, pp. 293–311. doi:10.1002/nme.1620260202

[25] Nashif, A. D., Jones, D. I. G., and Henderson, J. P., *Vibration Damping*, Wiley, New York, 1985.

[26] Jones, D. I. G., *Handbook of Viscoelastic Vibration Damping*, Wiley, New York, 2001.

[27] Daya, E. M., and Potier-Ferry, M., "A Numerical Method for Nonlinear Eigenvalue Problems Application to Vibrations of Viscoelastic Structures," *Computers and Structures*, Vol. 79, 2001, pp. 533–541. doi:10.1016/S0045-7949(00)00151-6

[28] Lee, D. H., and Hwang, W. S., "Length Optimization for Unconstrained Visco-Elastic Damping Layer of Beams," *The Transactions of the Korean Society for Noise and Vibration Engineering*, Vol. 13, No. 12, 2003, pp. 938–946.

[29] Garbow Burton, S., "The QZ Algorithm to Solve the Generalized Eigenvalue Problem for Complex Matrices," *ACM Transactions on Mathematical Software*, Vol. 4, No. 4, 1978, pp. 404–410. doi:10.1145/356502.356500

[30] Koo, B. U., "Shape Design Sensitivity Analysis of Acoustic Problems Using a Boundary Element Method," *Computers and Structures*, Vol. 65, No. 5, 1997, pp. 713–719. doi:10.1016/S0045-7949(96)00322-7

[31] Smith, D. C., and Bernhard, R. J., "Computation of Acoustic Shape Design Sensitivity Using a Boundary Element Method," *Journal of Vibration and Acoustics*, Vol. 114, Jan. 1992, pp. 127–132.

[32] Choi, K. K., Shim, I., and Wang, S., "Design Sensitivity Analysis of Structure-Induced Noise and Vibration," *Journal of Vibration and Acoustics*, Vol. 119, April 1997, pp. 173–179.

[33] Scarpa, F., "Parametric Sensitivity Analysis of Coupled Acoustic-Structural Systems," *Journal of Vibration and Acoustics*, Vol. 122, April 2000, pp. 109–115. doi:10.1115/1.568447

[34] Kim, N. H., Dong, J., Choi, K. K., Vlahopoulos, N., Ma, Z. D., Castanier, M. P., and Pierre, C., "Design Sensitivity Analysis for Sequential Structural-Acoustic Problems," *Journal of Sound and Vibration*, Vol. 263, 2003, pp. 569–591. doi:10.1016/S0022-460X(02)01067-2

[35] Nelson, R. B., "Simplified Calculation of Eigenvector Derivatives," *AIAA Journal*, Vol. 14, No. 9, 1976, pp. 1201–1205.

[36] Wang, S. M., and Choi, K. K., "Continuum Sizing Design Sensitivity Analysis of Eigenvectors Using Ritz Vectors," *Journal of Aircraft*, Vol. 31, No. 2, 1993, pp. 457–459.

[37] Choi, K. K., and Kim, N. H., *Structural Sensitivity Analysis and Optimization 1: Linear Systems*, Springer–Verlag, New York, 2005.

[38] Arora, J. S., *Introduction to Optimum Design*, McGraw–Hill, New York, 1988.

J. Samareh
Associate Editor